IL NUOVO CIMENTO **39 C** (2016) 398
DOI 10.1393/ncc/i2016-16398-2

COLLOQUIA: IWM-EC 2016

Studying correlations in $^{40}Ar + {}^{58}Fe$ with FAUST

L. HEILBORN(1)(2)(*), C. LAWRENCE(1)(2), A. B. MCINTOSH(1), M. D. YOUNGS(1) and S. J. YENNELLO(1)(2)

(1) *Cyclotron Institute, Texas A&M University - College Station, TX, USA*
(2) *Chemistry Department, Texas A&M University - College Station, TX, USA*

received 10 January 2017

Summary. — The recent detector upgrade of the Forward Array Using Silicon Technology (FAUST) is discussed along with novel implementation of energy, position and particle identification (PID) calibrations which solve challenges introduced by the position-sensitive nature of the new silicon detectors. A slight position-dependence of the energy deposited in the silicon detectors can be accounted for by using corrections derived from a ^{228}Th source calibration. The position will be calibrated by using α particles from a point-like source at the target position through a tungsten mask of precision-cut stripes, which was positioned on the front-plate of the FAUST array. The PID can be calibrated with equations based on the energies deposited in silicon and CsI detectors, which can be verified with the proton-alpha calibration beam used in the experiment. The status and prospects for these calibrations are discussed. Calibration runs and data from the $^{40}Ar + {}^{58}Fe$ reaction are shown.

1. – Introduction

The behavior of ground-state beta-stable nuclear material is fairly well understood, but extrapolation of the behavior to extreme neutron-proton content and to densities away from saturation density is far from established. Understanding the properties of nuclear material at extreme n-p content and extreme density is relevant in describing naturally occurring astrophysical environments [1]. Nuclear reactions allow the investigation of nuclear matter at these non-equilibrium values of pressure, temperature, density and asymmetry. These quantities are explorable via a variety of different observables in nuclear physics experiments. The focus of this experiment is a deeper understanding of the asymmetry term of the nuclear equation of state (nEoS) and the observable in this case was chosen to be the proton-proton (pp) correlation function. Because of the

(*) E-mail: lheilborn@comp.tamu.edu.

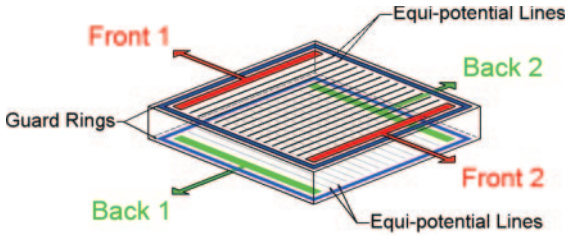

Fig. 1. – Schematic of DADL, showing the equipotential lines on the uniformly resistive surface, which allows position to be determined by charge splitting [6].

demonstrated sensitivity of pp correlation functions to spatial and temporal properties of the source, as well as the final-state interactions of the protons, the nEoS can be explored using this observable [2-4].

It is important to have excellent angular and energy resolution for the particles of interest when extracting correlation functions. For the purposes of this experiment, the Forward Array Using Silicon Technology (FAUST) was upgraded to improve position information. Data were collected from a variety of systems, which allowed for the variation of isospin asymmetry of the system while keeping either the total atomic mass or the total atomic number constant for two sets of comparisons. The reactions were 40 MeV/nucleon ^{40}Ar + ^{58}Fe, ^{40}Ar + ^{70}Zn and ^{40}Ca + ^{58}Ni, all run at the Texas A&M Cyclotron Institute. The status of current calibrations of data from the successful campaign with this position-sensitive upgrade are described here for the ^{40}Ar + ^{58}Fe system.

2. – Experimental apparatus

FAUST is comprised of sixty-eight ΔE-E telescopes positioned and gained for the detection of light charged particles (LCPs) emitted from the excited source resulting from heavy ion reactions [5]. Each telescope consists of a 2×2 cm 300 μm thick position-sensitive Dual-Axis Dual-Lateral (DADL) silicon diode backed by a CsI(Tl)-photodiode detector for ΔE-E identification of LCPs [6].

Figure 1 is a schematic of a DADL detector. The DADLs have uniform resistance across the front and back of the detectors and employ charge-splitting to determine the position of the detected charged particles to within 200 μm [6]. A reverse bias is applied to the silicon semiconductor which depletes the conduction band. Electrons and positive "holes", liberated by ionizing radiation, migrate to opposite faces of the detector due to the bias voltage. Because of the resistive surface across each face of the detector, the electrons on the back of the detector split proportionally into two back signals, while the resultant holes are charge split proportionally into two front signals. These four signals allow the relative x and y position of the detected fragment to be determined. The two front or two back signals are summed independently to determine the total energy, while the difference gives an indication of the position of the hit. Guard rings and conductive equipotential strips ensure a uniform potential across each surface of the detector [6]. The signals were then processed via high-gain preamplifiers and ASIC shaping amplifiers [7].

3. – Energy calibration

After signal processing, the addition of the two front or back signals gives the total energy deposited in the Si detector. A ^{228}Th source was used for energy calibrations. The

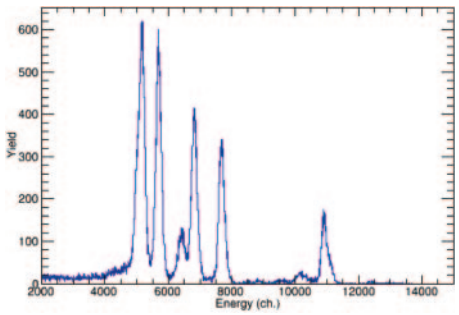

Fig. 2. – Raw energy spectrum of the alpha particles emitted by the ^{228}Th on detector 11. The E-calibrated Full-Width at Half Maximum (FWHM) is 300 keV for the highest energy α.

five dominant α energies of ^{228}Th and its daughters result in the raw spectrum shown in fig. 2. The position-dependence of the widths of these peaks was investigated by plotting the sum *vs.* the difference of the two front (or back) signals, which is a raw way of plotting the energy of the α particle against the one-dimensional (1D) position of the hit on the detector. The resultant two-dimensional (2D) histogram from the front signals is shown in fig. 3. These plots should be linear and horizontal, as the energies deposited by the single energy alpha particles should not be dependent upon the position of the incident radiation. This histogram is clearly curved, rather than flat, indicating that the response of the DADL detectors is not completely linear as a function of position on the detector face. The widths of the Gaussian peaks at each energy in fig. 2 are increased by some amount with the location of the α particle hit, due to incomplete charge collection.

A position-dependent correction improves the resolution of the raw energies before calibration. Each of the lines corresponding to an α particle energy from the ^{228}Th source were fit quadratically. So "a" represents the curvature of the line, "b" characterizes the asymmetry, and "c" tells the y-intercept. Where $x = 0$, the alpha particle hit the middle of the detector, and the measured values at $x = 0$ are used as a reference to which the values at other locations are mapped. The results of these fits are also depicted in fig. 3.

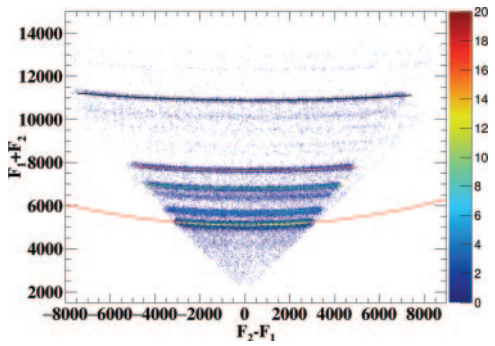

Fig. 3. – Sum *vs.* difference for ^{228}Th source α energies deposited in detector 11. These fits are somewhat parabolic in shape, and asymmetric about zero. Each line is fit quadratically. The highest energy alpha fit is black, followed, in order of decreasing energy, by red, green, blue and yellow lines of fit (color online).

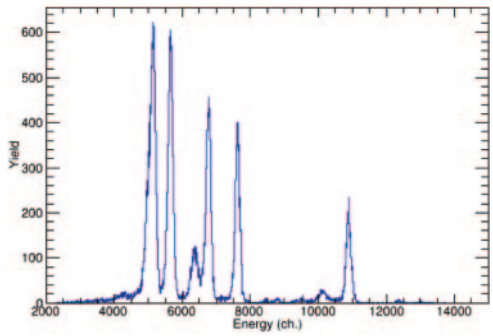

Fig. 4. – Corrected energy spectrum of the α particles emitted by the ^{228}Th source on detector 11. The FWHM is now 180 keV for the highest energy α, a significant improvement in resolution as compared to the original fig. 2.

The aim here is to remove any position-dependence of the energy. The curvature and linearity of the fits vary independently from one another, but in an approximately linear manner with the energy of the α particles. In this case, the "c" parameter of the fit is where the single-energy alpha line crosses the center of the detector, so it is some measure of the energy of the alpha particle. The non-linear components of this fit can be subtracted from the overall energy, to give a corrected spectrum and improve the energy resolution.

Because curvature and linearity are dependent upon the sum, or the c value, a and b can be replaced with linear functions that describe this relationship. Once these substitutions are made, the resultant equation for the corrected energy of any two front or back signals looks like this:

$$\text{Sum}_{\text{corr}} = \text{sum} - a(\text{sum})\text{diff}^2 - b(\text{sum})\text{diff}. \tag{1}$$

The resultant 1D energy spectrum, with improved resolution, is shown in fig. 4. The 2D histogram with the straightened, horizontal lines after the correction is made is shown in fig. 5. Once the position-dependence is accounted for, the peaks from the different energy alpha particles have much better resolution. The resulting position-corrected spectrum is shown in fig. 4. Even a merely cursory comparison between figs. 4 and 2, the spectrum before and after, shows that the resolution of the detector is much improved by this correction. This process has been implemented on all detectors. The known peaks of the α's in the thorium spectrum have been used to convert the position-corrected raw values into MeV.

Due to the thickness of the Si detectors, the α particles from the Th source do not punch into the CsI detectors. Higher energy α and proton-α beams accelerated to 15 MeV/nucleon and 10 MeV/nucleon, respectively, by the K500 Cyclotron were used for the purpose of calibrating the CsI. The CsI calibrations for LCPs also depend upon the PID, so are dependent upon the successful PID method described below.

4. – Position calibration

In addition to high positional accuracy of a detected particle within a detector, the relative alignment from one detector to another must be known in order to take full

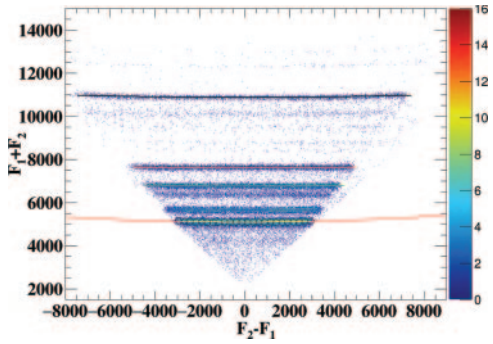

Fig. 5. – The sum *vs.* difference for the ^{228}Th α in detector 11 after implementation of position-dependent correction to energy deposition. Each line is a quadratic fit for a given α energy.

advantage of the angular resolution available with this upgrade. In order to calibrate relative detector position, a mask of 0.040″ thick tungsten was designed and produced. To prevent the large beam spot from effectively scattering elastic alpha particles around the slits in the mask, an aluminum collimator was used to reduce the effective source or beam spot to 1 mm.

A photograph of this mask is shown in fig. 6. Slits of 0.010″ were angled through the mask using wire electrical discharge machining (EDM) in order to allow α particles from a source or elastically scattered off of a ^{197}Au target to reach each detector in FAUST. The square cut through the center allows the beam to pass through, reducing beam particle intereactions with the tungsten mask. The stripes from the mask can be seen on the face of the detectors by gating on a single α energy from a thorium source or elastically scattered beam, the spectrum from a ^{228}Th α is shown in fig. 7.

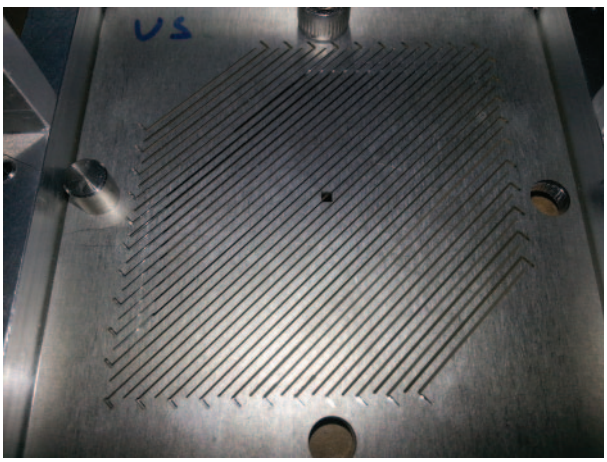

Fig. 6. – Mask as machined by sinker and wire EDM by Reliable EDM of Houston, Texas. Square hole in the center allows the beam to deposit into a faraday cup after the FAUST array.

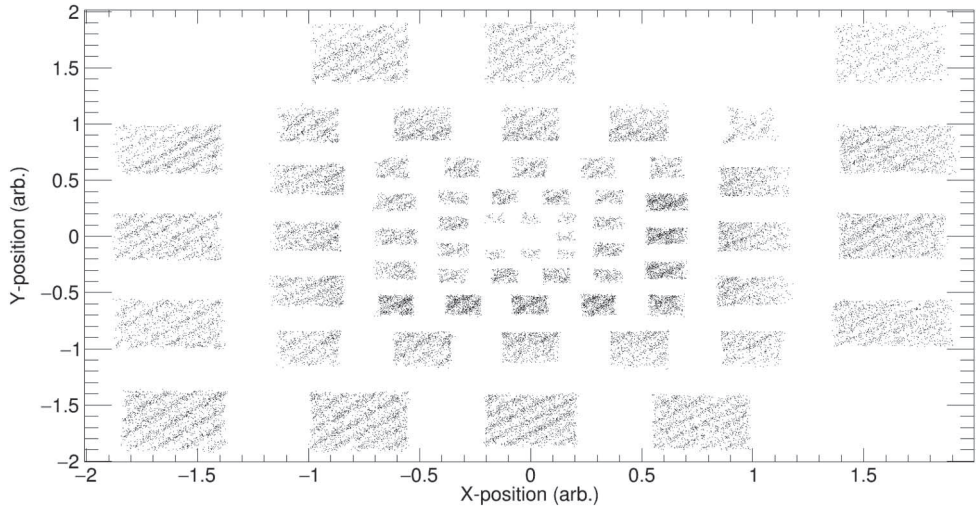

Fig. 7. – Position spectra of detectors, cut on the E of the highest energy ^{228}Th α in the silicons, through the position-calibration mask.

5. – Particle identification

The CsI energy calibration is dependent upon the particle identification (PID). The ΔE-E plot, derived from Si and CsI(Tl) signals, demonstrating the excellent differentiation between protons, deuterons and tritons for raw signals, is shown in fig. 8.

The PID values can be extracted using the following equation:

$$\text{PID} = b * \ln(p_0) - \ln(b * \Delta E) - (b-1)\ln(E + p_1 + \Delta E), \tag{2}$$

where b is defined as

$$b = p_2 - p_3 \frac{\Delta E}{p_4}, \tag{3}$$

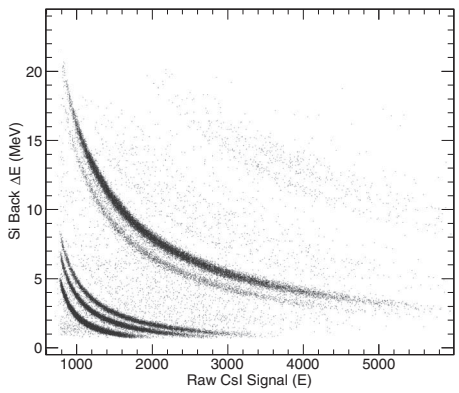

Fig. 8. – Representative ΔE-E plot, detector 52 for the reaction of 40 A MeV ^{40}Ar + ^{58}Fe.

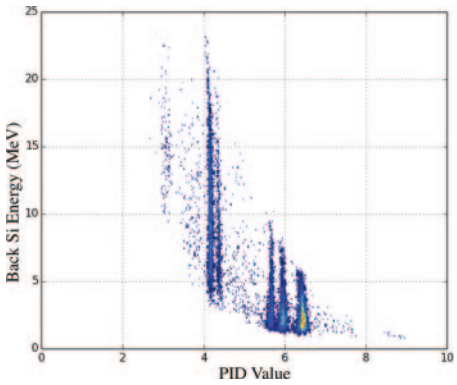

Fig. 9. – Detector 52, back ΔE *vs.* PID value, demonstrating the linearization of data from fig. 8 achievable via PID eq. (2).

and slopes and intercepts for the energy calibration of Si (ΔE) and CsI (E) are allowed to be free parameters. All fit parameters in eqs. (2) and (3) (p_0, p_1, p_2, p_3, p_4, b and the slopes and intercepts of the Si and CsI calibrations) are varied by hand while viewing PID *vs.* Si or PID *vs.* CsI as shown in fig. 9. The parameters result in the distribution of the PID *vs.* Si or PID *vs.* CsI being vertical bands when the free parameters are finalized. These parameters are allowed to vary for each detector.

After using the transformations of eqs. (2) and (3), ranges of the x-axis PID values in fig. 9 are then used to define the particle types.

6. – Conclusion

The energy and position calibrations of the data set described here are ongoing. Proton-proton correlation functions will be extracted and then compared to simulation results. In this manner, the impact of the asymmetry energy term of the equation of state on the shape and magnitude of the correlation function will be investigated.

* * *

This work was supported by the Robert A. Welch Foundation (Grant A-1266) and the United States Department of Energy (Grants DE-FG02-93ER40773 and DE-SC0004972). The Yennello group would like to acknowledge the excellent staff of the Cyclotron Institute at Texas A&M for the beam delivery and quality that made this work possible. Reliable EDM (6940 Fulton St, Houston, TX 77022) for manufacturing the position calibration mask. And Dick Todd of Riscorp (1706 Louisville Drive, Suite A2, Knoxville, TN 37921) for his work on design and manufacturing of the high-gain preamps used.

REFERENCES

[1] Baran V., Colonna M., Greco V. and Toro M. D., *Phys. Rep.*, **410** (2005) 335.
[2] Chen C. W., Greco V., Ko C. M. and Li B. A., *Phys. Rev. Lett.*, **90** (2003) 162701.
[3] Koonin S., *Phys. Lett. B*, **70** (1977) 43.

[4] Boal D. H., Gelbke C. and Jennings B. K., *Rev. Mod. Phys.*, **62** (1990) 553.
[5] Gimeno-Nogues F. *et al.*, *Nucl. Instrum. Methods Phys. Res. A*, **399** (1997) 94.
[6] Soisson S. N. *et al.*, *Nucl. Instrum. Methods Phys. Res. A*, **613** (2010) 240.
[7] Engel G. L., Sadasivam M., Nethi M., Elson J. M., Sobotka L. G. and Charity R. J., *Nucl. Instrum. Methods Phys. Res. A*, **573** (2007) 418.